International Journal of Mass Spectrometry 521 (2026) 117569

Contents lists available at ScienceDirect

International Journal of Mass Spectrometry

journal homepage: www.elsevier.com/locate/ijms

Advances in tapping-mode scanning probe electrospray ionization (t-SPESI): Instrumental development for high-spatial-resolution ambient mass spectrometry imaging

Yoichi Otsuka [a,b,c]

[a] Department of Physics, Graduate School of Science, Osaka University, 1-1 Machikaneyama-cho, Toyonaka, Osaka, 560-0043, Japan
[b] Forefront Research Center, Graduate School of Science, Osaka University, 1-1 Machikaneyama-cho, Toyonaka, Osaka, 560-0043, Japan
[c] Department of Chemistry, Graduate School of Science, Osaka University, 1-1 Machikaneyama-cho, Toyonaka, Osaka, 560-0043, Japan

ARTICLE INFO

Keywords:
Tapping-mode scanning probe electrospray ionization
Ambient sampling and ionization
Mass spectrometry imaging
Instrumentation development
Single-cell imaging

ABSTRACT

Mass spectrometry imaging (MSI) is an essential technique for visualizing the distribution of molecules in biological tissues. Ambient sampling ionization-based MSI has attracted attention for its ability to analyze samples directly; however, improving spatial resolution remains a major technical challenge. Young Scientist developed a tapping-mode scanning probe electrospray ionization (t-SPESI) method that uniquely combines the core technologies of electrospray ionization (ESI) and atomic force microscopy (AFM). By using an oscillating capillary probe to periodically supply minute amounts of solvent to the sample surface, t-SPESI enables spatiotemporal separation of the extraction and ionization processes, allowing rapid, soft ionization of analytes in micro-regions of the sample. In addition, the oscillating probe senses the sample surface, minimizing the influence of surface topography on extraction and ionization during MSI. Young Scientist has further advanced high-spatial-resolution t-SPESI-MSI through the development of feedback-control methods, probe fabrication techniques, and miniaturization of t-SPESI units. This paper provides an overview of the progress made in the development of t-SPESI instrumentation and highlights MSI results obtained from tissues and single cells.

1. Introduction

1.1. Mass spectrometry imaging for visualizing biomolecules

In living tissues, diverse cell types are spatially organized, and homeostasis is maintained through a series of highly regulated and interactive processes involving cell type-specific metabolic activities and the spatial distribution of metabolites, lipids, and proteins. Each cell exhibits diverse metabolic states depending on its differentiation stage and local microenvironment, and cellular heterogeneity within tissues is deeply involved in the onset and progression of various diseases [1,2]. Therefore, technologies that can elucidate spatially resolved metabolic and molecular states in tissues are essential for unveiling the integrated regulation of biomolecules [3–5].

Mass spectrometry imaging (MSI) is a powerful analytical technique for visualizing the spatial distribution of molecules in biological samples. By ionizing multiple molecules present within microregions of tissue sections and reconstructing ion peak information from the mass spectra, MSI enables simultaneous molecular identification and spatial mapping within cells. Unlike optical techniques such as fluorescence microscopy or Raman spectroscopy, MSI provides access to diverse biomolecules—including metabolites, lipids, and proteins—based on their high-accuracy molecular weight measurement, making it possible to analyze the metabolic states of cells and the chemical interactions between cells within diseased regions. Recent advancements have led to single-cell MSI (SC-MSI), enabling high-spatial-resolution visualization of components within individual cells [6–9].

In matrix-assisted laser desorption/ionization-based MSI (MALDI-MSI), a pulsed laser beam irradiates tissue sections covered with a microcrystalline matrix layer, causing simultaneous desorption and ionization of both the matrix and sample molecules [10]. This technique enables the analysis of a wide range of molecules, including lipids, metabolites, proteins, and N-glycans, and has been used to visualize cellular heterogeneity in diseased tissues, such as those affected by cancer [11,12] and neurological disorders [13–16]. Recent post-ionization approaches have further improved spatial resolution,

This article is part of a special issue entitled: Young Scientist Features published in International Journal of Mass Spectrometry.

E-mail address: otsuka@phys.sci.osaka-u.ac.jp.

https://doi.org/10.1016/j.ijms.2025.117569
Received 23 November 2025; Received in revised form 22 December 2025; Accepted 28 December 2025
Available online 29 December 2025

enabling single-cell and subcellular MSI [17–19]. However, MALDI-MSI faces inherent limitations. The crystal size and thickness of the matrix layer on the tissue sections affect the extraction/ionization efficiency and spatial resolution of MSI [20–22]. Consequently, ambient mass spectrometry (AMS), which enables direct matrix-free analysis, has attracted increasing attention.

1.2. *Development of direct analytical techniques utilizing electrospray ionization*

AMS employs a technique that directly samples and ionizes samples with little or no pretreatment under ambient conditions. Its key features include enabling rapid analysis and minimizing variations in component distribution caused by sample pretreatment. Since the early 2000s, various methods for AMS have been developed for the direct analysis of biological samples [23–31]. Among them, ionization techniques capable of analyzing microregions can be applied to MSI.

Desorption electrospray ionization (DESI) is a representative commercialized technique in which a charged solvent at a high voltage flows through the inner tube of a coaxial capillary sprayer, while nitrogen gas flows from the outer tube to accelerate the charged droplets [32,33]. When a stream of charged droplets generated by electrospray ionization (ESI) [34] is sprayed onto a sample surface, the analyte molecules are locally dissolved and extracted from the sample. The resulting extracts are desorbed with the charged droplets, and ions are generated during the droplet-drying process. MSI using DESI (DESI-MSI) can be performed by scanning the sample in two dimensions while keeping the sprayer stationary. Miniaturization of the spray diameter and solvent flow rate has enabled high-spatial-resolution DESI-MSI with pixel sizes as small as 5 μm [33]. DESI-MSI has become a useful method for matrix-free visualization of lipids and metabolites in biological tissues [35] and enables detection of molecular species distinct from those detected by MALDI-MSI [36].

In nanospray DESI (nano-DESI), two capillaries are arranged in a V-shape; a primary capillary supplies a high-voltage solvent, while a secondary capillary collects the solvent. When the liquid bridge between the capillaries contacts the sample surface, a microscale liquid bridge forms, and the sample components are extracted. The extract is then subjected to ESI at the tip of the secondary capillary [37]. The ion source is commercially available in China but not globally. The microscale liquid bridge enables high-spatial-resolution MSI of tissues at sub-10 μm resolution. Furthermore, to suppress changes in the liquid bridge caused by surface unevenness, a shear force probe is positioned between the two capillaries. Changes in its oscillation amplitude are monitored, enabling feedback control to stabilize the formation of liquid bridge [38–40].

Although DESI enables high-spatial-resolution MSI, completely eliminating the influence of sample surface unevenness or tilt remains challenging. In contrast, nano-DESI can extract sample components via a liquid bridge while suppressing the effects of surface unevenness.

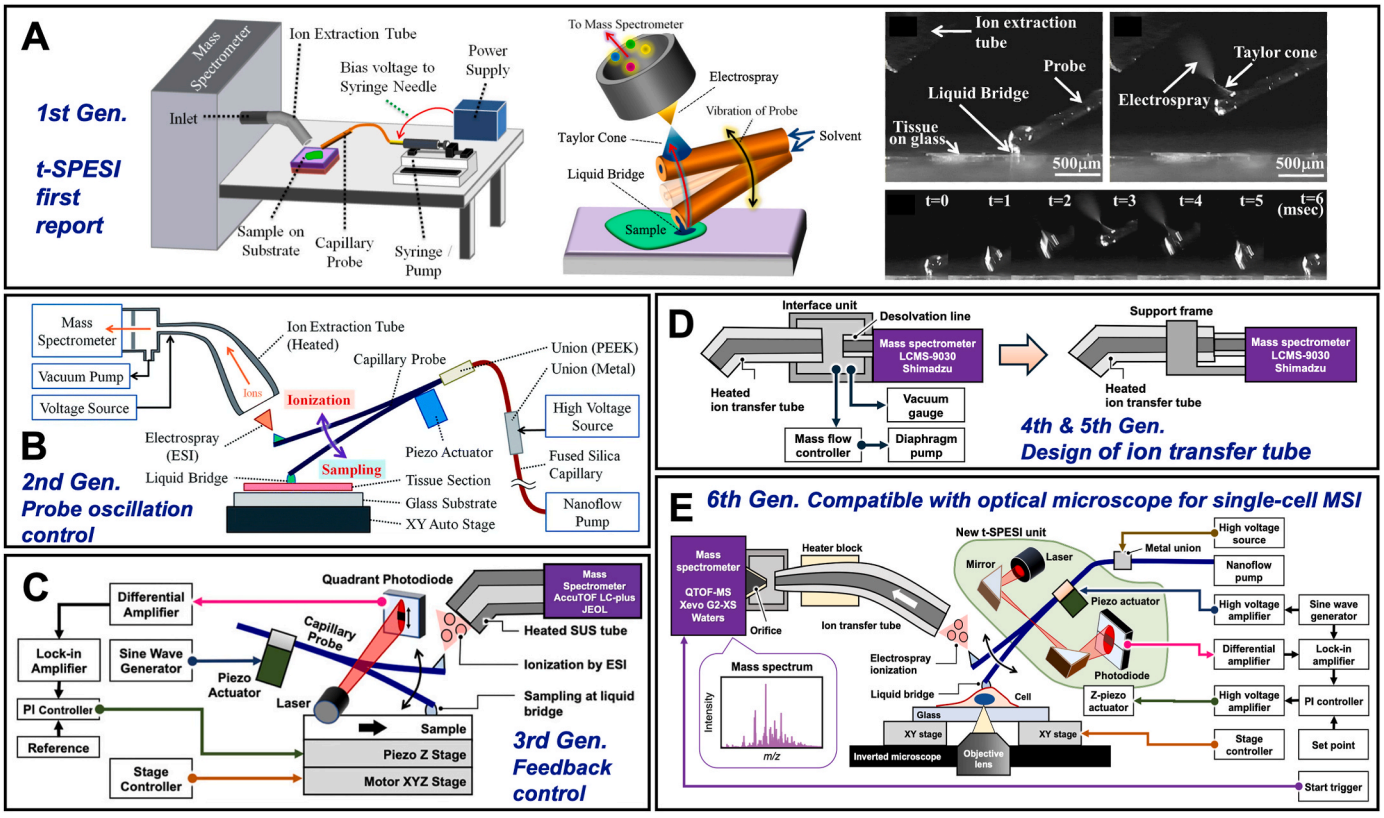

Fig. 1. Schematic of t-SPESI measurement systems developed to date. (A) First-generation system: Local extraction ionization at the probe tip was demonstrated using spontaneous vertical oscillations of the solvent-flowing probe. High-speed camera observations revealed that the extraction and ionization processes were spatiotemporally separated. *Rapid Commun. Mass Spectrom.* **26** (2012) 2725–2732. Reproduced with permission from John Wiley and Sons. (B) Second-generation system: By fixing the probe to a piezo actuator, extraction-ionization can be performed by controlling the oscillation frequency of the probe. *Analyst* **139** (2014) 2336–2341. Copyright 2014 The Royal Society of Chemistry. (C) Third-generation system: Probe-shadow displacement was measured using a laser beam, photodiode, differential amplifier, and lock-in amplifier. A feedback control method was developed to dynamically adjust the height of the sample stage and maintain a constant oscillation amplitude during probe scanning. *Anal. Chem.* **93** (2021) 2263–2272. Copyright 2021 American Chemical Society. (D) Fourth-generation and Fifth-generation system: Ion detection sensitivity was improved by directly connecting the ion transport tube to the mass spectrometer inlet. *Anal. Bioanal. Chem.* **417** (2025) 275–286. Copyright 2025 Springer Nature. (E) Sixth-generation system: A compact t-SPESI unit was developed for use with an inverted optical microscope. SC-MSI of HeLa cells on a glass substrate was demonstrated using a sharpened silica bead-filled probe. *Commun. Chem.* **8** (2025) 147. Copyright 2025 Springer Nature.

However, the size of the liquid bridge depends on the spatial arrangement of the probe, which can sometimes limit the spatial resolution.

2. Progress in the development of tapping-mode scanning probe electrospray ionization (t-SPESI)

2.1. Proposal of t-SPESI

In 2012, we proposed scanning probe electrospray ionization (SPESI), an ambient ionization technique (Fig. 1A) [41]. In SPESI, a charged solvent is locally supplied to the sample surface using a single capillary probe. Analytes are extracted via a liquid bridge formed between the probe and sample, and the resulting extract is directly subjected to ESI as the probe is periodically displaced vertically relative to the sample surface.

The idea for SPESI originated from an accidental observation. While conducting experiments with a homemade DESI device, the author noticed spontaneous vertical oscillation of the capillary, reminiscent of the motion of a cantilever which is used in atomic force microscopy (AFM). During his PhD studies, the author developed nanoscale measurement techniques using AFM [42,43], which commonly operates in two modes: tapping mode, where an oscillating probe intermittently contacts the sample surface, and contact mode, where a stationary probe remains in continuous contact with the sample.

Based on this insight, the author hypothesized that intermittently tapping an oscillating probe against a sample could enable simultaneous extraction and ionization at the probe tip. By adjusting the position of the tissue section and probe and performing tapping with the probe, multiple ion peaks appeared in the mass spectra, representing the first proof-of-concept of tapping-mode scanning probe electrospray ionization (t-SPESI). Inspired by AFM operation modes, a technique called contact-mode SPESI (c-SPESI) was also devised, in which the probe remains fixed and the sample side oscillates using an ultrasonic transducer to promote ESI.

In both methods, high-speed camera observations confirmed the formation of a liquid bridge and onset of electrospraying at the probe tip. In t-SPESI, when the oscillating probe tip contacts the sample surface, a liquid bridge forms between the two; as the probe moves away from the sample, this bridge breaks, forming a Taylor cone that generates an electrospray. t-SPESI introduces the novel concept of spatiotemporally separating extraction and ionization using the oscillation of a single probe. However, in the initial demonstration, t-SPESI relied on spontaneous probe oscillation, making precise control of the oscillation difficult.

2.2. Demonstration of MSI using t-SPESI

After proposing the concept of t-SPESI for AMS, a new measurement system was constructed to perform MSI using t-SPESI (t-SPESI-MSI) [44]. A mechanism was developed for attaching the probe to a piezoelectric actuator, enabling excitation at any desired frequency. In addition, an automated stage equipped with a stepper motor was incorporated to enable two-dimensional scanning of the sample (Fig. 1B). Control programs for the actuator and stage were developed in LabVIEW. Using this system, MSI was performed on mouse brain tissue sections mounted on glass slides to visualize the characteristic lipid distributions in regions such as the cerebral cortex, corpus callosum, and caudate-putamen. This study marks the first demonstration of t-SPESI-MSI.

2.3. Stabilization of sampling and ionization by feedback control and demonstration of multimodal imaging

In t-SPESI, periodic probe–sample contact drives analyte extraction and ionization. In practice, however, samples are not ideally flat, the surfaces of the tissue sections are uneven, and the sample stage often exhibit a slight tilt. Therefore, as the probe scans the sample, the oscillation amplitude varies depending on surface topology. In protruded or indented areas, the probe–sample distance decreases or increases, causing the amplitude to decrease or increase, respectively. Such fluctuations alter the contact time between the probe and the sample, potentially leading to variations in extraction and ionization efficiency during t-SPESI-MSI.

To address this issue, we developed a feedback control system that measures the oscillation amplitude of the probe and maintains it constant (Fig. 1C) [45]. A laser beam is directed at the side of the capillary probe, and the transmitted light is detected using a segmented photodiode. The differential signal between the photodiodes is used to monitor probe-shadow displacement in real time. The oscillation amplitude is measured using a lock-in amplifier, and a proportional-integral (PI) controller calculates an error signal to match the measured amplitude to the setpoint values. This error signal is then sent to the z-stage controller to adjust the sample height. The feedback control system effectively minimized the influence of surface tilt and unevenness, maintaining a constant probe oscillation amplitude during scanning.

Because the feedback error signal reflects the surface shape, recording it during MSI provides simultaneous acquisition of both ion images and sample topography. t-SPESI-MSI of mouse brain tissue visualized the distribution of hexosylceramides and phosphatidylethanolamine with a spatial resolution of approximately 6.5 μm (Fig. 2A–C). The acquisition of topography and amplitude images confirmed proper operation of the feedback control system (Fig. 2D and E).

2.4. Effects of probe oscillation frequency on MSI

In t-SPESI-MSI, it is necessary to bring the probe close to the sample surface to perform tapping. Although feedback control can maintain a constant oscillation amplitude during the probe scanning, it is essential to understand the interaction between the probe tip and sample during the approach process. Therefore, inspired by a force-curve analysis used in AFM, we developed a measurement system to investigate how the oscillation amplitude and phase change with probe oscillation frequency during the approach [46,47].

The oscillation amplitude during approach varied significantly depending on the oscillation frequency and polarity of the applied voltage. In the positive-ion mode, significant changes in amplitude and phase were observed as the probe approached the tissue section. In the negative-ion mode, fluctuations in amplitude and phase were minimal, enabling more stable tapping operation.

The amplitude response in the positive-ion mode differed depending on whether the oscillation frequency was lower or higher than the resonance frequency. These behaviors were attributed to frequency shifts caused by attractive electrostatic interactions between the probe tip and the surface of tissue section. We found that using a lower oscillation frequency than the resonant frequency stabilized the approach, whereas at higher frequency than the resonant frequency, stable approach was not possible and MSI could not perform reliably. These results demonstrate that appropriate adjustment of the probe oscillation frequency is critical for t-SPESI-MSI.

2.5. Development of ion transfer tubes to improve ion detection sensitivity

In t-SPESI, a metallic ion transfer tube is used to introduce ions generated at the probe tip into the mass spectrometer. In a previous t-SPESI system, a small homemade chamber served as an intermediary between the ion transfer tube and the MS inlet, with ions introduced by evacuating the chamber (Fig. 1D). Inside this chamber, a ~1 mm gap existed between the ion transfer tube and MS inlet, raising concerns that ions or charged droplets could scatter within this gap, decreasing the introduction efficiency of the analytes into the mass spectrometer.

To address this issue, we designed an interface that directly

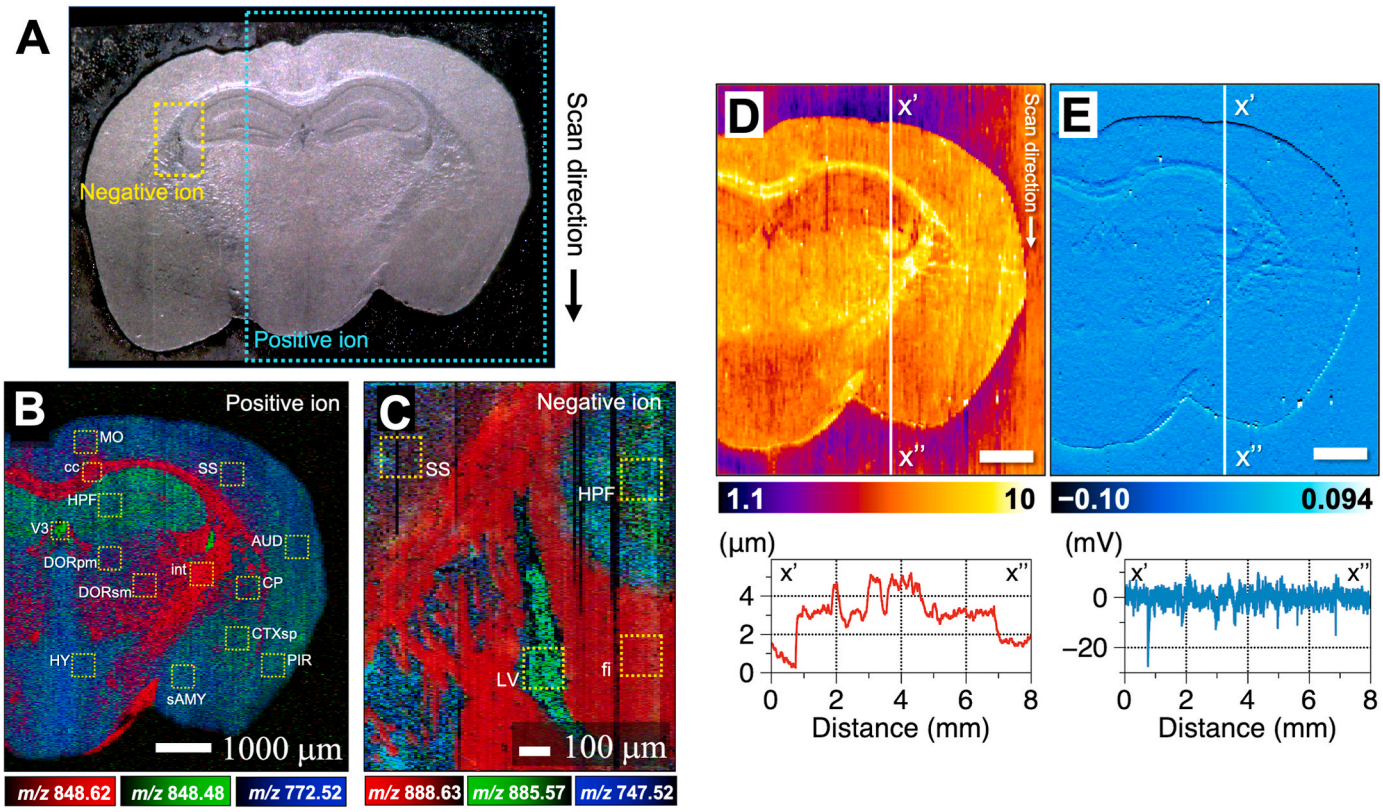

Fig. 2. MSI of mouse brain sections using a third-generation t-SPESI system. While implementing feedback control to maintain a constant probe oscillation amplitude, the distribution of phospholipids in mouse brain tissue (A) was visualized in both positive-ion (B) and negative-ion modes (C). Through feedback control, the topography (D) of the tissue section and amplitude images (E) were acquired simultaneously with MSI. This demonstrated that the probe's oscillation amplitude could be maintained despite the unevenness of the sample surface. *Anal. Chem.* **93** (2021) 2263–2272. Copyright 2021 American Chemical Society.

connected the ion transfer tube to the MS inlet [48]. Using this direct-connection configuration, the signal intensity of the NaI cluster ions increased on average, more than fourfold in the positive-ion mode and approximately 1.5-fold in the negative-ion mode. Further evaluation using a rhodamine B film confirmed that shortening the ion transfer tube (from 24 to 11 mm) improved the signal intensity per pixel by an average factor of 2.6.

2.6. Development of a measurement system for single-cell MSI

To realize single-cell MSI (SC-MSI), which enables the visualization of molecular distributions within individual cells, the extraction area must be reduced to the micron scale, which is one order of magnitude smaller than typical cell dimensions. Furthermore, precise alignment of the probe and the cells requires integration with a microscope. Thus, we focused on developing a probe capable of stable delivery of minute solvent volumes and a compact t-SPESI unit compatible with an inverted optical microscope (Fig. 1E) [49].

The capillary probe was fabricated using a laser puller (P-2000, Sutter, USA). However, as the tip-opening diameter decreases, contamination and particles in the solvent often clog the probe, preventing solvent delivery to the target. To address this, we filled the probe with porous silica particles commonly used in liquid chromatography–mass spectrometry (LC–MS). This approach prevents clogging and improves solvent delivery stability.

For the new t-SPESI unit, we integrated a laser light source, probe oscillation unit, photodiode unit, and two mirrors to guide the laser beam into a compact housing. The t-SPESI unit was placed above the sample stage of an inverted microscope without interference. Supported by a z-direction piezo stage, the height of the unit was adjusted in real time through feedback control while maintaining a constant oscillation amplitude of the probe during measurement. Using an inverted microscope, we observed the position and size of the liquid bridge on the glass substrate from the rear and aligned the relative positions of the probe tip and cells. This system enabled multimodal imaging, which allowed the acquisition of fluorescent images, ion images, and topography of HeLa cells in the same field of view.

2.7. Brief summary of t-SPESI development

As described above, t-SPESI development has progressed through several key stages: (1) proposal of the operating principle, (2) stabilization of probe oscillation, and (3) improvement of ion detection sensitivity and spatial resolution for MSI (Table 1). The probe-oscillation strategy, oscillation-amplitude feedback control, silica particle-filled probe, and compact t-SPESI unit developed thus far constitute essential foundational technologies enabling high-spatial-resolution MSI of tissues and single cells.

In particular, developing a measurement method for probe oscillation for feedback control took considerable time. First, we adopted a method similar to AFM, where a laser beam was irradiated onto the probe surface and the displacement of the reflected beam was detected using a segmented photodiode [50]. The problem with this method was that adjusting the positions of the laser beam and photodiode became complicated. Therefore, we devised a method to measure the probe shadow and designed and developed an optical system. Furthermore, to implement MSI, the development of multiple fundamental technologies was required, including probe oscillation control, sample stage control, oscillation measurement, and feedback control. The author advanced both the hardware design and software development.

Table 1
Summary of t-SPESI System Development.

System Generation	Year	Instrumentation update	Mass spectrometer	Targets	Reference
1st	2012	First report of t-SPESI	TSQ 7000 (Thermo Fisher Scientific)	Insulin, BSA, mouse pancreas	[41]
2nd	2014	Probe oscillation with piezo actuator	QSTAR XL (AB Sciex)	Rat brain	[44]
3rd	2021	Optical detection of probe oscillation Feedback control of sample stage	AccuTOF (JEOL)	Mouse brain	[45]
4th	2023, 2024	Update mass spectrometer	LCMS-9030 (Shimadzu)	Solvent effect Oscillation frequency effect	[46,52]
5th	2025	Direct connection of ion transfer tube	LCMS-9030 (Shimadzu)	Mouse testes	[48]
6th	2025	Compact t-SPESI unit compatible with an inverted microscope Silica bead-filled probe	Xevo G2-XS (Waters)	HeLa cells	[49]

3. Application of t-SPESI-MSI to bioanalysis

3.1. Visualization of metabolites, lipids, and proteins in mouse pancreatic cancer

To demonstrate the applicability of t-SPESI to biological tissues, MSI was performed on mouse pancreatic cancer tissues generated by injecting human pancreatic carcinoma cell lines (Fig. 3A–C) using the 2nd generation system [51]. Fresh-frozen tissue sections were mounted on glass slides and analyzed without pretreatment. Measurements were performed in positive-ion mode using a solvent mixture of methanol/water/formic acid (50:50:1, v/v). Ion signals of spermine, phosphocholine, phosphatidylcholine (PC) 34:2, and PC 36:4 were tentatively assigned in the cancerous region, whereas spermidine showed a higher intensity in the non-cancerous region (Fig. 3D and E). These results suggested that polyamine metabolism and phospholipid synthesis were regulated in cancerous tissues. Furthermore, multiple ion peaks were detected as multiply charged species in the *m/z* range of 800–1500. Deconvolution analysis of these peaks enabled tentative assignment of thymosin β10 (4936.6 Da), thymosin β4 (4963.6 Da), calcyclin (S100A6, 10090.6 Da), and calpactin I light chain (S100A10, 11072.1 Da), all of which exhibited markedly higher signal localization in the cancerous region (Fig. 3F and G). In this study, we demonstrated that polyamines, lipids, and proteins can be simultaneously detected and that their heterogeneous distribution within the cancer tissue can be directly visualized. These findings highlight the potential of t-SPESI as a valuable tool for cancer metabolism and biomarker research.

3.2. Solvent effects in t-SPESI-MSI of mouse brain tissue

The physicochemical properties of the solvents used in t-SPESI are expected to influence the extraction-ionization efficiency and spatial resolution of MSI. Therefore, we systematically investigated the effects of solvent polarity, viscosity, and surface tension on MSI performance using the 4th generation system [52]. t-SPESI-MSI was performed on mouse brain tissue sections in positive-ion mode using a mixed solvent of *N,N*-dimethylformamide (DMF)/methanol (1:1, v/v) —a mixture known to permit extraction and ionization without damaging biological tissues [53]—as well as each pure solvent.

Across all solvent conditions, 93 lipids were putatively assigned, and the signal intensity and image contrast were compared for each brain region. When DMF was used alone, the spatial resolution decreased, likely due to the low transfer efficiency of the extract to the electrospray despite DMF's high lipid solubility. Furthermore, being an aprotic solvent, DMF suppressed lipid protonation. In contrast, when methanol was used alone, the signal intensity decreased compared with that obtained

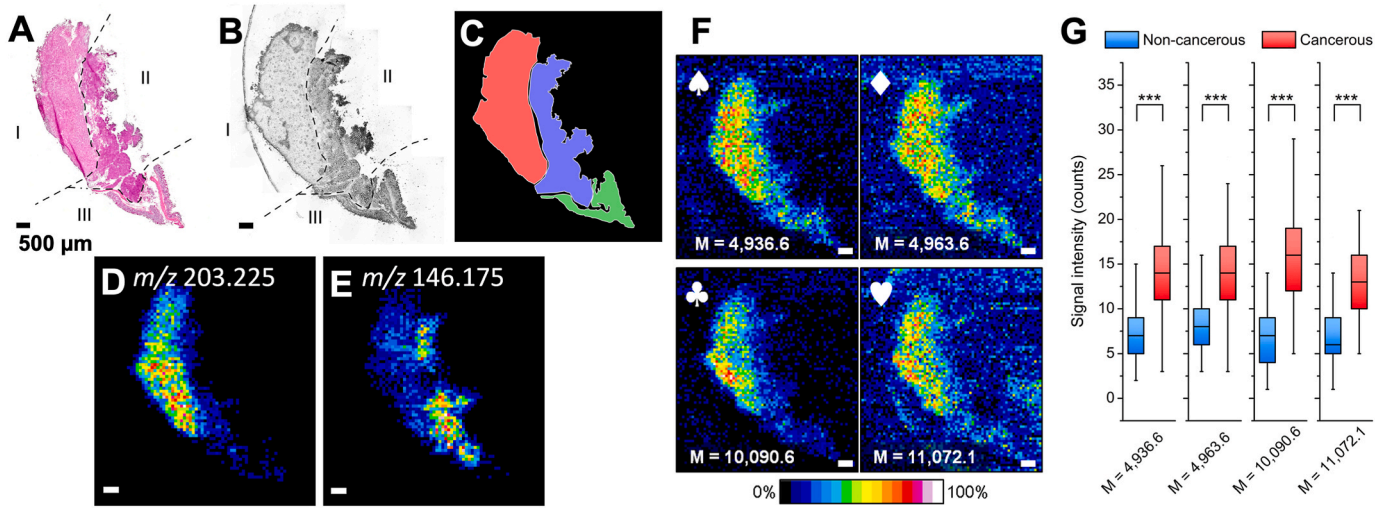

Fig. 3. MSI of a mouse pancreatic cancer tissue section using the second-generation t-SPESI system. (A) Optical microscope image of adjacent tissue sections stained with H/E. (B) Optical microscope image of the unstained tissue sections used for MSI. (C) Schematic showing cancerous (red) and non-cancerous (blue) regions determined from H/E staining. (D, E) Ion images of metabolites: *m/z* 203.225 and *m/z* 146.175 were putative protonated molecules of spermine and spermidine, respectively, and showed increased signal intensities in cancerous and non-cancerous regions. (F) Ion images of four multiply charged protein ions. Deconvolution of multivalent ion peaks suggested the presence of thymosin beta (Tβ) 10 (4936.6 Da), Tβ4 (4963.6 Da), calcyclin (S100-A6, 10090.6 Da), and calpactin I light chain (S100-A10, 11072.1 Da) in the sample. These proteins showed increased signal intensity in the cancerous region. (G) Comparison of signal intensities between cancerous and non-cancerous regions revealed significant differences. *J. Mass Spectrom.* **50** (2015) 1157–1162. Copyright (2015) John Wiley and Sons. (For interpretation of the references to colour in this figure legend, the reader is referred to the Web version of this article.)

with the mixed solvent, although the transfer efficiency was high and small charged droplets were generated; however, methanol's lipid solubility was lower than that of DMF. The 1:1 DMF/methanol mixture resulted in intermediate properties, providing a good balance between the ion signal intensity and spatial resolution.

As mentioned in the previous section, mixed solvents containing aqueous solutions are potentially effective for metabolite and protein ionization. Investigating the relationship between solvent properties and extraction-ionization using the approach outlined herein would be crucial for solvent design.

3.3. Visualization of localized lipids in mouse testes

Lysophosphatidic acid acyltransferase 3 (LPLAT3) is a primary enzyme that synthesizes phospholipids containing docosahexaenoic acid (DHA-PL) by incorporating DHA into phospholipids. The high flexibility of DHA-PL enhances the deformability and vesicle-forming ability of cell membranes, thereby promoting endocytosis. In mouse testes, DHA-PL contributes to the function and transport of various proteins required for sperm release and serves as a metabolic precursor for DHA-derived lipid mediators. Although LPLAT3 deficiency impairs spermatogenesis by disrupting DHA-PL synthesis [54], the detailed distribution of these lipids within tissues remains unclear.

Tissue sections of wild-type (WT) and LPLAT3 knockout (KO) mouse testes were examined in positive-ion mode with a pixel size of 5 μm using the 5th generation system (Fig. 4) [48]. Using a probe with an inner tip diameter of approximately 4 μm, a DMF/methanol mixed solvent (1:1, v/v) was delivered at a flow rate of 5 nL/min using a nanoflow pump. To compare the distribution of cells and lipids in the testes, optical images of hematoxylin and eosin (H/E)-stained tissue sections were examined alongside MSI ion images. Lipid ions were assigned by referencing previously reported LC-MS/MS data.

The convoluted seminiferous tubules (CST) of mouse testes exhibit a layered structure, with cell distribution changing as spermatogenesis progresses. t-SPESI-MSI of WT mouse testes clearly visualized lipid distributions corresponding to these structures. PC 34:1 localized to the outer periphery of CST, whereas PC 36:1 was localized in the stromal region outside the CST. Notably, PC 38:6—a representative DHA-PL—showed high intensity within the inner CST and was primarily localized to the cytoplasm of Sertoli cells (Fig. 4A–D). Conversely, in KO mice, the PC 38:6 signal was markedly reduced and its distribution was unclear, although PC 34:1 and PC 36:1 distributions resembled those of WT testes (Fig. 4E–H). This change in spatial distribution clearly demonstrates that DHA-PL deficiency in the inner CST originates within the Sertoli cell layer, supporting the hypothesis that LPLAT3 is responsible for local DHA-PL production during spermatogenesis. These results highlight the value of t-SPESI-MSI for investigating lipid metabolism in genetically modified mouse tissues.

3.4. Visualization of lipids in HeLa cells

Single-cell MSI of HeLa cells was performed using the 6th generation t-SPESI measurement system integrated with an inverted fluorescence microscope [49]. HeLa mCAT and IP-cGCS cells were cultured on glass substrates; the latter cell line overexpresses glucosylceramide synthase (GCS). After chemical fixation, the HeLa cells were stained with fluorescent dyes (Hoechst 33342 and FDA) and dried (Fig. 5A). MSI was performed in the positive ion mode with a pixel size of 2 μm using a probe with a tip inner diameter of approximately 2 μm. Mass spectra were acquired over the *m/z* range of 100–1200 with a 300 ms accumulation time. Lipid ions were identified by referencing the results of supercritical fluid chromatography-tandem mass spectrometry (SFC-MS/MS).

Statistical analysis of the MSI data revealed significant differences ($p < 0.005$) in the signal intensities of the 29 lipid ions between HeLa mCAT and IP-cGCS cells (Fig. 5B). Principal component analysis showed clear separation between the two cell types based on lipid metabolic characteristics (Fig. 5C). Ion images of PC 34:2 and PC 38:4 displayed strong signals in the cytoplasm and plasma membrane, whereas the nuclear region showed reduced signal intensity (Fig. 5D, G). In contrast, the sphingomyelin (SM) species—SM d18:1/22:0, SM d18:1/18:2, and SM d18:1/16:0—exhibited diffuse distributions over each cell without strong regional localization, consistent with expected membrane-wide distribution (Fig. 5E, F, H) The ion images of hexosylceramide (HexCer) revealed increased signal intensity in cGCS cells, characterized by high expression of glycolipid-synthesizing enzymes (Fig. 5I).

This study demonstrated, for the first time, the applicability of t-SPESI to SC-MSI and achieved visualization of intracellular lipid localization in HeLa cells. t-SPESI-SC-MSI is expected to serve as a powerful cell analysis tool for investigating metabolic changes during the cell cycle or drug treatments.

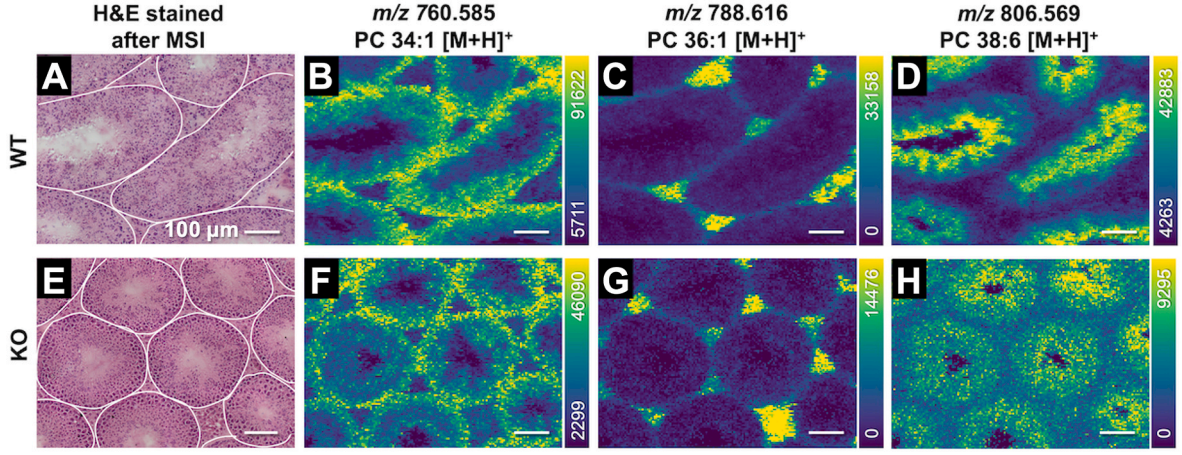

Fig. 4. MSI of mouse testis sections using a fifth-generation t-SPESI system. Comparison of optical microscope and lipid ion images. (A) Optical microscope image of H/E-stained WT mouse testis after MSI. (B–D) Comparison of ion images of WT mouse testes. In the PC 34:1 $[M + H]^+$ image, the intensity increased in the CST outer regions relative to that of the inner regions, indicating that PC 34:1 was distributed more in the regions corresponding to spermatogonia and spermatocytes. The PC 36:1 $[M + H]^+$ image showed the localization of the signal in the stromal region outside CSTs. In the PC 38:6 $[M + H]^+$ (DHA-PL) image, the intensity increased inside CST. (E) Optical microscopy of H/E-stained LPLAT3 KO mouse testes after MSI. (F–H) Comparison of ion images in KO mouse testes. The PC 34:1 $[M + H]^+$ and PC 36:1 $[M + H]^+$ images resembled those of the WT testes; however, their signal intensities were lower. In contrast, the intensity of PC 38:6 $[M + H]^+$ inside CST was significantly lower than that in WT testes. *Anal. Bioanal. Chem.* **417** (2025) 275–286. Copyright 2025 Springer Nature.

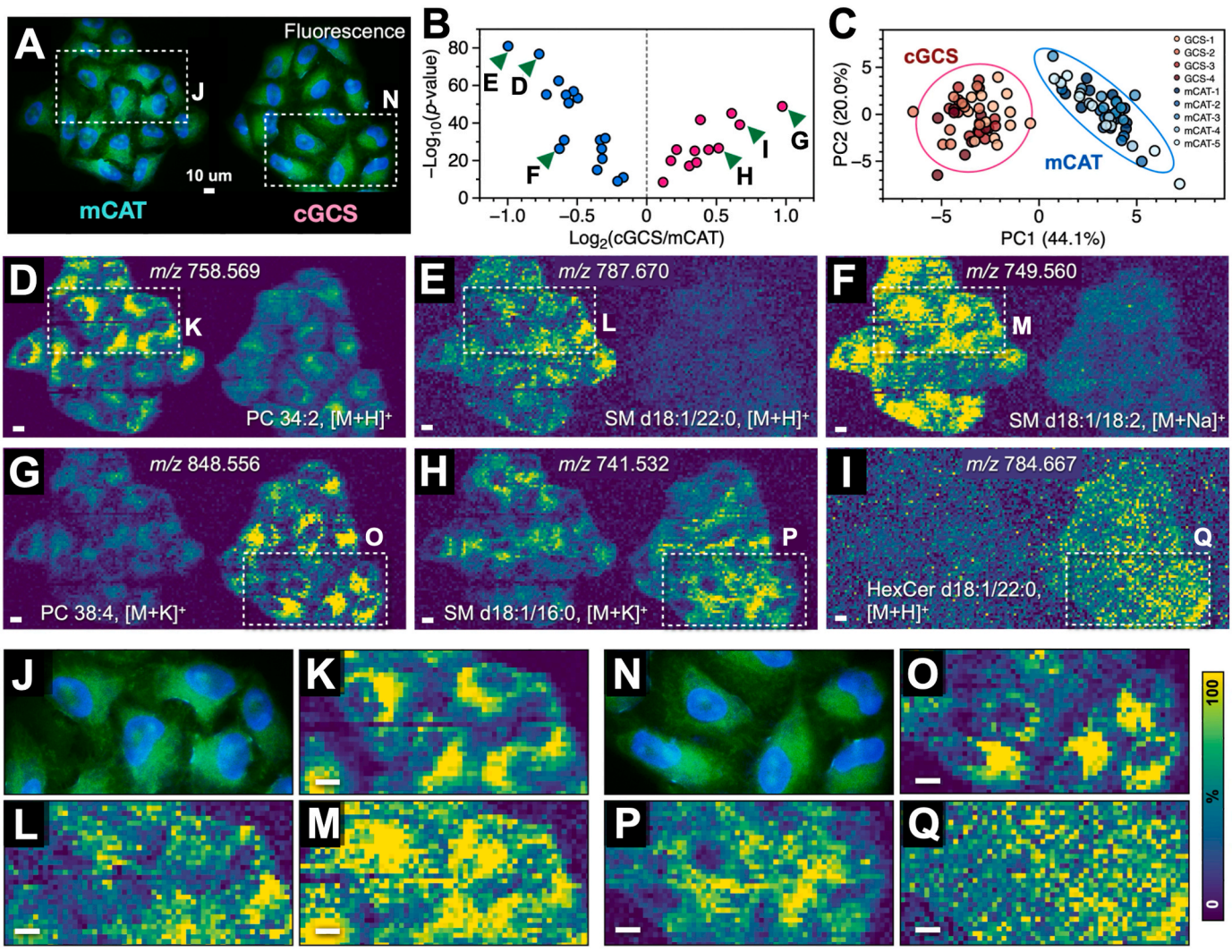

Fig. 5. MSI of HeLa cells using a 6th generation t-SPESI system. (A) Fluorescence images of mCAT and cGCS cells. (B) Volcano plot showing the differences in the signal intensities of lipid ions between cell types. The signal intensities of 29 lipid ions were used ($p < 0.005$). (C) Score plot obtained by principal component analysis, showing two distinct groups with 95 % confidence ellipses. Ion images with high signal intensities in mCAT cells (D–F) and cGCS cells (G–I). Enlarged fluorescence and ion images showing a high signal intensity in mCAT (J–M) and cGCS (N–Q) cells. The enlarged regions are indicated by the dashed lines. *Commun. Chem.* **8** (2025) 147. Copyright 2025 Springer Nature.

4. Conclusion and future perspectives

This review summarizes the development and applications of t-SPESI. The oscillating probe in t-SPESI not only separates analyte extraction and electrospray ionization in space and time—enabling rapid ambient sampling and ionization—but also functions as a surface sensing element. Through feedback control of the oscillation amplitude, it is possible to dynamically compensate for the effects of sample surface unevenness on the destabilization of the extraction and ionization processes of the analytes. This multifunctionality fundamentally distinguishes t-SPESI from conventional continuous-extraction ambient ionization techniques. Through the development of core technologies for high-spatial-resolution MSI, we successfully demonstrated matrix-free SC-MSI. The use of a DMF/MeOH mixed solvent prevented the disappearance of cells in the tissue sections after MSI. The combination of MSI and tissue staining is effective for verifying the correlation between cell components and morphology.

To further improve the analytical performance of t-SPESI-MSI, it is necessary to integrate it with diverse techniques that have been actively developed within the MSI community. Over the past two decades, MSI has evolved through the incorporation of post-ionization, on-tissue chemical derivatization, fragmentation and/or ion mobility separation, and sample preparation strategies such as tissue expansion.

Recent studies have demonstrated substantial improvements in ion detection sensitivity by post-ionization techniques using lasers, plasma, and VUV in MALDI- and DESI-based imaging platforms [17,18,55–57]. Post-ionization plays a complementary role by converting the neutral species that escape primary ionization into detectable ions. Incorporating post-ionization abilities into the ion transfer tube is expected to enhance the molecular coverage and ionization efficiency of t-SPESI-MSI.

On-tissue chemical derivatization has also emerged as a powerful approach for enhancing the detection sensitivity and molecular coverage of MSI. In conventional MALDI-MSI, derivatization is performed across entire tissue sections to improve the ionization of specific biomolecules [58]. In contrast, ambient techniques such as DESI and nano-DESI can induce in situ reactions for rapid, localized labeling of low-polarity molecules while preserving spatial information [59–63]. Recent studies have demonstrated that photochemical or charge-labeling reactions using solvent-phase reagents can selectively target functional groups and improve structural discrimination. Because t-SPESI can utilize derivatization reagent solutions similar to DESI and

nano-DESI, it is well positioned to expand the molecular information accessible in SC-MSI.

Tandem mass spectrometry (MS/MS) and ion mobility spectrometry (IMS) provide orthogonal dimensions for molecular characterization that can significantly enhance the structural specificity of MSI. In the MS/MS configuration, the mass spectra of the fragment ions provide fingerprints for more reliable assignments [64,65], while IMS offers an additional separation dimension based on the gas-phase collision cross section (CCS), which reflects the molecular size, shape, and charge distribution [66–68]. Together, MS/MS and IMS provide complementary structural insights; hybrid approaches enable comprehensive molecular annotation, improve confidence in compound identification, and provide a deeper understanding of chemical heterogeneity in tissues [69]. The coupling of MS/MS and/or IMS with t-SPESI is therefore expected to advance the accuracy of SC-MSI.

Furthermore, recent developments in tissue expansion techniques have opened new avenues for improving the apparent spatial resolution of MSI without modifying analytical instrumentation. By embedding biological samples in polymer matrices and physically enlarging them under controlled conditions, molecular distributions can be visualized with enhanced spatial fidelity while preserving the native chemical composition [70–73]. Combining t-SPESI with expanded tissues may enable submicrometer-equivalent MSI, providing deeper insights into cellular and subcellular organization.

Quantitative MSI is needed not only for studying diseased tissues but also for its application in pharmacological studies. To achieve quantitative measurements using ESI-based extraction-ionization techniques, technology that ensures a stable solvent flow during the extraction process is essential. We demonstrated that solvent delivery using a nanoflow pump and minimizing the influence of sample surface morphology using feedback control were effective for stabilizing the formation of minute liquid bridges. However, further development of stabilization techniques is necessary. The solution we most urgently require is a pump system capable of stable solvent delivery with sub-nanoliter resolution per minute and pressure monitoring. To our knowledge, no commercially available pump meets this optimal requirement. Superior delivery technology will be key to enabling the widespread application of single-cell t-SPESI-MSI across diverse research targets.

Moving forward, our research will continue with a dual focus on instrument development and its application to diseased tissues. We will address key challenges, including further miniaturization of the extraction area, improvements in sensitivity and stability of the system, to upgrade t-SPESI-MSI into a versatile, next-generation ambient MSI platform. By visualizing the heterogeneity of cellular networks in diseased tissues with high precision, we aim to contribute meaningfully to advances in life science research.

Funding sources

Current research projects on device development and mass spectrometry imaging of diseased tissues are supported by JSPS KAKENHI (grant numbers JP23H03711 and JP23K17880), JST PRESTO (grant number JPMJPR20E4), Nakatani Foundation, Shimadzu Science Foundation, Asahi Glass Foundation, Toyota Riken Scholar Program, and Terumo Life Science Foundation.

Declaration of competing interest

The author has declared no conflict of interest.

Acknowledgments

The author expresses sincere gratitude to all collaborators, students, and colleagues who have contributed to the development of t-SPESI over the years. The constructive discussions, dedicated experimental work, and creative ideas provided by laboratory members are invaluable. The author also thanks Professors Takuya Matsumoto and Michisato Toyoda at the University of Osaka for their guidance and support throughout this research.

Data availability

Data will be made available on request.

References

[1] D.A. Lawson, K. Kessenbrock, R.T. Davis, N. Pervolarakis, Z. Werb, Tumour heterogeneity and metastasis at single-cell resolution, Nat. Cell Biol. 20 (2018) 1349–1360, https://doi.org/10.1038/s41556-018-0236-7.
[2] F. Lüönd, S. Tiede, G. Christofori, Breast cancer as an example of tumour heterogeneity and tumour cell plasticity during malignant progression, Br. J. Cancer 125 (2021) 164–175, https://doi.org/10.1038/s41416-021-01328-7.
[3] J. De Jonghe, J.W. Opzoomer, A. Vilas-Zornoza, B.S. Nilges, P. Crane, M. Vicari, H. Lee, D. Lara-Astiaso, T. Gross, J. Morf, K. Schneider, J. Cudini, L. Ramos-Mucci, D. Mooijman, K. Tiklová, S.M. Salas, C.M. Langseth, N.D. Kashikar, E.M. Carrami, R. McIntyre, C.B. Swerner, E.M. Hessel, C.-A. Kapourani, C. Regep, C.E.S. Roberts, D. Schapiro, J. Lundeberg, M. Nilsson, A.K. Shalek, A.P. Cribbs, J.P. Taylor-King, scTrends: a living review of commercial single-cell and spatial 'omic technologies, Cell Genomics 4 (2024) 100723, https://doi.org/10.1016/j.xgen.2024.100723.
[4] C. Quek, A. Pratapa, X. Bai, G. Al-Eryani, I. Pires da Silva, A. Mayer, N. Bartonicek, K. Harvey, N.G. Maher, J.W. Conway, R.J. Kasalo, B. Ben Cheikh, O. Braubach, U. Palendira, R.P.M. Saw, J.R. Stretch, K.F. Shannon, A.M. Menzies, R.A. Scolyer, G.V. Long, A. Swarbrick, J.S. Wilmott, Single-cell spatial multiomics reveals tumor microenvironment vulnerabilities in cancer resistance to immunotherapy, Cell Rep. 43 (2024) 114392, https://doi.org/10.1016/j.celrep.2024.114392.
[5] J. Le, Y. Dian, D. Zhao, Z. Guo, Z. Luo, X. Chen, F. Zeng, G. Deng, Single-cell multiomics in cancer immunotherapy: from tumor heterogeneity to personalized precision treatment, Mol. Cancer 24 (2025) 221, https://doi.org/10.1186/s12943-025-02426-3.
[6] H. Zhang, D.G. Delafield, L. Li, Mass spectrometry imaging: the rise of spatially resolved single-cell omics, Nat. Methods 20 (2023) 327–330, https://doi.org/10.1038/s41592-023-01774-6.
[7] M.J. Taylor, J.K. Lukowski, C.R. Anderton, Spatially resolved mass spectrometry at the single cell: recent innovations in proteomics and metabolomics, J. Am. Soc. Mass Spectrom. 32 (2021) 872–894, https://doi.org/10.1021/jasms.0c00439.
[8] L. Xing, C.-L. Zhao, H.-Z. Mou, J. Pan, B. Kang, H.-Y. Chen, J.-J. Xu, Next generation of mass spectrometry imaging: from micrometer to subcellular resolution, Chemical & Biomedical Imaging 1 (2023) 670–682, https://doi.org/10.1021/cbmi.3c00061.
[9] H. Zhang, K.H. Lu, M. Ebbini, P. Huang, H. Lu, L. Li, Mass spectrometry imaging for spatially resolved multi-omics molecular mapping, Npj Imaging 2 (2024) 20, https://doi.org/10.1038/s44303-024-00025-3.
[10] R.M. Caprioli, T.B. Farmer, J. Gile, Molecular imaging of biological samples: localization of peptides and proteins using MALDI-TOF MS, Anal. Chem. 69 (1997) 4751–4760, https://doi.org/10.1021/ac970888i.
[11] J.P. Hartig, K. Bejar, L.E.A. Young, G. Grimsley, J.R. Bethard, D.A. Troyer, J. Hernandez, J.D. Wu, J.E. Ippolito, L.E. Ball, J.A.L. Gelfond, T.L. Johnson-Pais, A. S. Mehta, R.J. Leach, P.M. Angel, R.R. Drake, Determining the N-Glycan and Collagen/extracellular matrix protein compositions in a novel outcome cohort of prostate cancer tissue microarrays using MALDI-MSI, Cancer Res. Commun. 4 (2024) 3036–3048, https://doi.org/10.1158/2767-9764.CRC-24-0152.
[12] K.D. Duncan, H. Pětrošová, J.J. Lum, D.R. Goodlett, Mass spectrometry imaging methods for visualizing tumor heterogeneity, Curr. Opin. Biotechnol. 86 (2024) 103068, https://doi.org/10.1016/j.copbio.2024.103068.
[13] Q. Zhang, Y. Li, P. Sui, X.-H. Sun, Y. Gao, C.-Y. Wang, MALDI mass spectrometry imaging discloses the decline of sulfoglycosphingolipid and glycerophosphoinositol species in the brain regions related to cognition in a mouse model of Alzheimer's disease, Talanta 266 (2024) 125022, https://doi.org/10.1016/j.talanta.2023.125022.
[14] D. Jha, K. Blennow, H. Zetterberg, J.N. Savas, J. Hanrieder, Spatial neurolipidomics—MALDI mass spectrometry imaging of lipids in brain pathologies, J. Mass Spectrom. 59 (2024), https://doi.org/10.1002/jms.5008.
[15] Y. Chen, D. Hu, L. Zhao, W. Tang, B. Li, Unraveling metabolic alterations in transgenic mouse model of Alzheimer's disease using MALDI MS imaging with 4-aminocinnoline-3-carboxamide matrix, Anal. Chim. Acta 1192 (2022), https://doi.org/10.1016/j.aca.2021.339337.
[16] N. Ollen-Bittle, S. Pejhan, S.H. Pasternak, C.D. Keene, Q. Zhang, S.N. Whitehead, Co-registration of MALDI-MSI and histology demonstrates gangliosides co-localize with amyloid beta plaques in Alzheimer's disease, Acta Neuropathol. 147 (2024) 105, https://doi.org/10.1007/s00401-024-02759-1.
[17] A. Potthoff, J. Schwenzfeier, M. Niehaus, S. Bessler, E. Hoffmann, O. Soehnlein, J. Höhndorf, K. Dreisewerd, J. Soltwisch, Spatial biology using single-cell mass spectrometry imaging and integrated microscopy, Nat. Commun. 16 (2025) 9129, https://doi.org/10.1038/s41467-025-64603-8.
[18] R.S.E. Young, A.-K. Piper, L. McAlary, J.C. McKinnon, J.S. Lum, J. Soltwisch, M. Niehaus, S.R. Ellis, Subcellular mass spectrometry imaging of lipids and nucleotides using transmission geometry ambient laser desorption and plasma ionisation, Nat. Commun. 16 (2025) 9130, https://doi.org/10.1038/s41467-025-64604-7.

[19] M. Niehaus, J. Soltwisch, M.E. Belov, K. Dreisewerd, Transmission-mode MALDI-2 mass spectrometry imaging of cells and tissues at subcellular resolution, Nat. Methods 16 (2019) 925–931, https://doi.org/10.1038/s41592-019-0536-2.
[20] A.A. Patil, M.J.N. Descanzo, V.B. Dhisale, W.-P. Peng, MALDI sample preparation methods: a mini review, Int. J. Mass Spectrom. 498 (2024) 117219, https://doi.org/10.1016/j.ijms.2024.117219.
[21] T. Mahamdi, C.G. Serna, R. Giné, J. Rofes, S.A. Mohammed, P. Ràfols, X. Correig, M. García-Altares, C. Hopf, S.-A. Iakab, O. Yanes, Improving MALDI mass spectrometry imaging performance: Low-temperature thermal evaporation for controlled matrix deposition and improved image quality, J. Am. Soc. Mass Spectrom. 36 (2025) 1100–1110, https://doi.org/10.1021/jasms.5c00015.
[22] T.-H. Hahm, W. Wang, D.R. Brown, C.M. Tressler, S.C. Kuo, K. Glunde, MALDI matrix sublimation versus spray coating in the FluoMALDI imaging pipeline, Anal. Chim. Acta 1376 (2025) 344610, https://doi.org/10.1016/j.aca.2025.344610.
[23] J. Laskin, I. Lanekoff, Ambient mass spectrometry imaging using direct liquid extraction techniques, Anal. Chem. 88 (2016) 52–73, https://doi.org/10.1021/acs.analchem.5b04188.
[24] M.Z. Huang, S.C. Cheng, Y.T. Cho, J. Shiea, Ambient ionization mass spectrometry: a tutorial, Anal. Chim. Acta 702 (2011) 1–15, https://doi.org/10.1016/j.aca.2011.06.017.
[25] R. Javanshad, A.R. Venter, Ambient ionization mass spectrometry: real-time, proximal sample processing and ionization, Anal. Methods 9 (2017) 4896–4907, https://doi.org/10.1039/c7ay00948h.
[26] S.C. Cheng, C. Shiea, Y.L. Huang, C.H. Wang, Y.T. Cho, J. Shiea, Laser-based ambient mass spectrometry, Anal. Methods 9 (2017) 4924–4935, https://doi.org/10.1039/c7ay00997f.
[27] J. Xue, Y. Bai, H. Liu, Recent advances in ambient mass spectrometry imaging, TrAC, Trends Anal. Chem. 120 (2019) 115659, https://doi.org/10.1016/j.trac.2019.115659.
[28] Y. Xiao, J. Deng, Y. Yao, L. Fang, Y. Yang, T. Luan, Recent advances of ambient mass spectrometry imaging for biological tissues: a review, Anal. Chim. Acta 1117 (2020) 74–88, https://doi.org/10.1016/j.aca.2020.01.052.
[29] S. Rankin-Turner, J.C. Reynolds, M.A. Turner, L.M. Heaney, Applications of ambient ionization mass spectrometry in 2021: an annual review, Anal. Sci. Adv. 3 (2022) 67–89, https://doi.org/10.1002/ansa.202100067.
[30] Y. Otsuka, Direct liquid extraction and ionization techniques for understanding multimolecular environments in biological systems (secondary publication), Mass Spectrom. 10 (2021) A0095, https://doi.org/10.5702/massspectrometry.A0095. A0095.
[31] A. Henderson, L.M. Heaney, S. Rankin-Turner, Advancements in ambient ionisation mass spectrometry in 2024: an annual review, Anal. Sci. Adv. 6 (2025), https://doi.org/10.1002/ansa.70007.
[32] Z. Takáts, J.M. Wiseman, B. Gologan, R.G. Cooks, Mass spectrometry sampling under ambient conditions with desorption electrospray ionization, Science 306 (2004) 471–473, https://doi.org/10.1126/science.1104404.
[33] M.W. Towers, R.J. DeHoog, T.M. Godfrey, L.A. Towers, E.A. Jones, J.B. Ballantyne, J.W. Suliburk, L.S. Eberlin, Development of low-flow high-resolution desorption electrospray ionization mass spectrometry imaging, J. Am. Soc. Mass Spectrom. (2025), https://doi.org/10.1021/jasms.5c00279.
[34] J.B. Fenn, M. Mann, C.K. Meng, S.F. Wong, C.M. Whitehouse, Electrospray ionization for mass spectrometry of large biomolecules, Science 246 (1989) 64–71, https://doi.org/10.1126/science.2675315.
[35] H. Liu, S. Huang, L. Yang, Y. He, Y. Jing, Y. Xie, B. Hu, Z. Li, H. Bi, Z. Li, The application of desorption electrospray ionization mass spectrometry and mass spectrometry imaging in metabolomics, lipidomics and proteomics analysis, Talanta 297 (2025) 128611, https://doi.org/10.1016/j.talanta.2025.128611.
[36] R. Joshi, S.Y. Tang, U.S. Das, D.J. Boehmler, A. Mrčela, R. Lordan, E.J. Petersson, A.M. Weljie, G.A. FitzGerald, Multimodal landscape of atherosclerotic plaques: a spatial omics approach with mass spectrometry imaging, Anal. Chim. Acta 1379 (2025) 344723, https://doi.org/10.1016/j.aca.2025.344723.
[37] J. Laskin, B.S. Heath, P.J. Roach, L. Cazares, O.J. Semmes, Tissue imaging using nanospray desorption electrospray ionization mass spectrometry, Anal. Chem. 84 (2012) 141–148, https://doi.org/10.1021/ac2021322.
[38] M. Yang, X. Tang, M. Iqfath, E. Hernly, D. Unsihuay, P. Manchanda, K. Sharma, Z. Qu, H. Hu, C. Beveridge, G. Chopra, J. Laskin, Multimodal Nano-DESI mass spectrometry imaging reveals phospholipids accumulation in and around amyloid plaques in alzheimer's disease, ACS Chem. Neurosci. 16 (2025) 3127–3137, https://doi.org/10.1021/acschemneuro.5c00144.
[39] R. Yin, K.E. Burnum-Johnson, X. Sun, S.K. Dey, J. Laskin, High spatial resolution imaging of biological tissues using nanospray desorption electrospray ionization mass spectrometry, Nat. Protoc. 14 (2019) 3445–3470, https://doi.org/10.1038/s41596-019-0237-4.
[40] S.N. Nguyen, R.L. Sontag, J.P. Carson, R.A. Corley, C. Ansong, J. Laskin, Towards high-resolution tissue imaging using nanospray desorption electrospray ionization mass spectrometry coupled to shear force microscopy, J. Am. Soc. Mass Spectrom. 29 (2018) 316–322, https://doi.org/10.1007/s13361-017-1750-8.
[41] Y. Otsuka, S. Shide, J. Naito, M. Kyogaku, H. Hashimoto, R. Arakawa, Scanning probe electrospray ionization for ambient mass spectrometry, Rapid Commun. Mass Spectrom. 26 (2012) 2725–2732, https://doi.org/10.1002/rcm.6399.
[42] Y. Otsuka, Y. Naitoh, T. Matsumoto, T. Kawai, A nano tester: a new technique for nanoscale electrical characterization by point-contact current-imaging atomic force microscopy, Jpn. J. Appl. Phys. 41 (2002) L742–L744, https://doi.org/10.1143/JJAP.41.L742.
[43] Y. Otsuka, Y. Naitoh, T. Matsumoto, T. Kawai, Point-contact current-imaging atomic force microscopy: measurement of contact resistance between single-walled carbon nanotubes in a bundle, Appl. Phys. Lett. 82 (2003) 1944–1946, https://doi.org/10.1063/1.1563308.
[44] Y. Otsuka, J. Naito, S. Satoh, M. Kyogaku, H. Hashimoto, R. Arakawa, Imaging mass spectrometry of a mouse brain by tapping-mode scanning probe electrospray ionization, Analyst 139 (2014) 2336–2341, https://doi.org/10.1039/C3AN02340K.
[45] Y. Otsuka, B. Kamihoriuchi, A. Takeuchi, F. Iwata, S. Tortorella, T. Matsumoto, High-spatial-resolution multimodal imaging by tapping-mode scanning probe electrospray ionization with feedback control, Anal. Chem. 93 (2021) 2263–2272, https://doi.org/10.1021/acs.analchem.0c04144.
[46] M. Sun, Y. Otsuka, M. Okada, S. Shimma, M. Toyoda, Probe oscillation control in tapping-mode scanning probe electrospray ionization for stabilization of mass spectrometry imaging, Analyst 149 (2024) 4011–4019, https://doi.org/10.1039/D4AN00712C.
[47] B. Kamihoriuchi, Y. Otsuka, A. Takeuchi, F. Iwata, T. Matsumoto, Visualization of sampling and ionization processes in scanning probe electrospray ionization mass spectrometry, Mass Spectrom. 7 (2019) S0078, https://doi.org/10.5702/massspectrometry.S0078. S0078.
[48] Y. Otsuka, M. Okada, T. Hashidate-Yoshida, K. Nagata, M. Yamada, M. Goto, M. Sun, H. Shindou, M. Toyoda, Improved ion detection sensitivity in mass spectrometry imaging using tapping-mode scanning probe electrospray ionization to visualize localized lipids in mouse testes, Anal. Bioanal. Chem. 417 (2025) 275–286, https://doi.org/10.1007/s00216-024-05641-x.
[49] Y. Otsuka, K. Kabayama, A. Miura, M. Takahashi, K. Hata, Y. Izumi, T. Bamba, K. Fukase, M. Toyoda, Single-cell mass spectrometry imaging of lipids in HeLa cells via tapping-mode scanning probe electrospray ionization, Commun. Chem. 8 (2025) 147, https://doi.org/10.1038/s42004-025-01521-2.
[50] Y. Otsuka, Tapping-mode scanning probe electrospray ionization: fusion of SPM with mass spectrometry, Jpn. J. Appl. Phys. 60 (2021) SE0802, https://doi.org/10.35848/1347-4065/abefac.
[51] Y. Otsuka, S. Satoh, J. Naito, M. Kyogaku, H. Hashimoto, Visualization of cancer-related chemical components in mouse pancreas tissue by tapping-mode scanning probe electrospray ionization mass spectrometry, J. Mass Spectrom. 50 (2015) 1157–1162, https://doi.org/10.1002/jms.3634.
[52] Y. Otsuka, N. Ote, M. Sun, S. Shimma, O. Urakawa, S. Yamaguchi, T. Kudo, M. Toyoda, Solvent effects of *N* , *N* -dimethylformamide and methanol on mass spectrometry imaging by tapping-mode scanning probe electrospray ionization, Analyst 148 (2023) 1275–1284, https://doi.org/10.1039/D2AN01953A.
[53] L.S. Eberlin, C.R. Ferreira, A.L. Dill, D.R. Ifa, L. Cheng, R.G. Cooks, Nondestructive, histologically compatible tissue imaging by desorption electrospray ionization mass spectrometry, Chembiochem 12 (2011) 2129–2132, https://doi.org/10.1002/cbic.201100411.
[54] Y. Iizuka-Hishikawa, D. Hishikawa, J. Sasaki, K. Takubo, M. Goto, K. Nagata, H. Nakanishi, H. Shindou, T. Okamura, C. Ito, K. Toshimori, T. Sasaki, T. Shimizu, Lysophosphatidic acid acyltransferase 3 tunes the membrane status of germ cells by incorporating docosahexaenoic acid during spermatogenesis, J. Biol. Chem. 292 (2017) 12065–12076, https://doi.org/10.1074/jbc.M117.791277.
[55] C. Liu, K. Qi, L. Yao, Y. Xiong, X. Zhang, J. Zang, C. Tian, M. Xu, J. Yang, Z. Lin, Y. Lv, W. Xiong, Y. Pan, Imaging of polar and nonpolar species using compact desorption electrospray ionization/postphotoionization mass spectrometry, Anal. Chem. 91 (2019) 6616–6623, https://doi.org/10.1021/acs.analchem.9b00520.
[56] K. Qi, Y. Lv, Y. Xiong, C. Tian, C. Liu, Y. Pan, Development of transmission ambient pressure laser desorption ionization/postphotoionization mass spectrometry imaging, Anal. Chem. 96 (2024) 5489–5498, https://doi.org/10.1021/acs.analchem.3c05605.
[57] A. Potthoff, K. Dreisewerd, J. Soltwisch, Detailed characterization of the postionization efficiencies in MALDI-2 as a function of relevant input parameters, J. Am. Soc. Mass Spectrom. 31 (2020) 1844–1853, https://doi.org/10.1021/jasms.0c00072.
[58] C. Harkin, K.W. Smith, F.L. Cruickshank, C. Logan Mackay, B. Flinders, R.M. A. Heeren, T. Moore, S. Brockbank, D.F. Cobice, On-tissue chemical derivatization in mass spectrometry imaging, Mass Spectrom. Rev. 41 (2022) 662–694, https://doi.org/10.1002/mas.21680.
[59] C. Wu, D.R. Ifa, N.E. Manicke, R.G. Cooks, Rapid, direct analysis of cholesterol by charge labeling in reactive desorption electrospray ionization, Anal. Chem. 81 (2009) 7618–7624, https://doi.org/10.1021/ac901003u.
[60] D. Lostun, C.J. Perez, P. Licence, D.A. Barrett, D.R. Ifa, Reactive DESI-MS imaging of biological tissues with dicationic ion-pairing compounds, Anal. Chem. 87 (2015) 3286–3293, https://doi.org/10.1021/ac5042445.
[61] L. Zhang, Y. Huang, Y. Zhou, Q. Wu, Y. Wang, H. Lu, Photocatalytic reactive liquid microjunction surface sampling-mass spectrometry for rapid and selective in-situ analysis of alpha-unsubstituted amine metabolites or drugs in brain tissue, J. Chromatogr. A 1696 (2023) 463958, https://doi.org/10.1016/j.chroma.2023.463958.
[62] J. Zhang, Q. Zang, W. Xu, F. Tang, Rapid imaging of unsaturated lipids at isomer level using photoepoxidation, Talanta 261 (2023) 124643, https://doi.org/10.1016/j.talanta.2023.124643.
[63] S. Amer, D. Unsihuay, M. Yang, J. Laskin, Universal photosensitizer for isomer-selective lipid imaging with high molecular coverage, Anal. Chem. 97 (2025) 7071–7078, https://doi.org/10.1021/acs.analchem.4c05538.
[64] A. Bednařík, V. Prysiazhnyi, D. Bezdeková, J. Soltwisch, K. Dreisewerd, J. Preisler, Mass spectrometry imaging techniques enabling visualization of lipid isomers in biological tissues, Anal. Chem. 94 (2022) 4889–4900, https://doi.org/10.1021/acs.analchem.1c05108.
[65] X. Guo, W. Cao, X. Fan, Z. Guo, D. Zhang, H. Zhang, X. Ma, J. Dong, Y. Wang, W. Zhang, Z. Ouyang, Tandem mass spectrometry imaging enables high definition

for mapping lipids in tissues, Angew. Chem. Int. Ed. 62 (2023), https://doi.org/10.1002/anie.202214804.
[66] K.V. Djambazova, D.R. Klein, L.G. Migas, E.K. Neumann, E.S. Rivera, R. Van de Plas, R.M. Caprioli, J.M. Spraggins, Resolving the complexity of spatial lipidomics using MALDI TIMS imaging mass spectrometry, Anal. Chem. 92 (2020) 13290–13297, https://doi.org/10.1021/acs.analchem.0c02520.
[67] D. Leontyev, H. Olivos, B. Shrestha, P.M. Datta Roy, M.C. LaPlaca, F.M. Fernández, Desorption electrospray ionization cyclic ion mobility-mass spectrometry imaging for traumatic brain injury spatial metabolomics, Anal. Chem. 96 (2024) 13598–13606, https://doi.org/10.1021/acs.analchem.4c02394.
[68] L.-X. Jiang, E. Hernly, H. Hu, R.T. Hilger, H. Neuweger, M. Yang, J. Laskin, Nanospray desorption electrospray ionization (Nano-DESI) mass spectrometry imaging with high ion mobility resolution, J. Am. Soc. Mass Spectrom. 34 (2023) 1798–1804, https://doi.org/10.1021/jasms.3c00199.
[69] S. Heuckeroth, A. Behrens, C. Wolf, A. Fütterer, I.D. Nordhorn, K. Kronenberg, C. Brungs, A. Korf, H. Richter, A. Jeibmann, U. Karst, R. Schmid, On-tissue dataset-dependent MALDI-TIMS-MS2 bioimaging, Nat. Commun. 14 (2023) 7495, https://doi.org/10.1038/s41467-023-43298-9.
[70] L.-C. Chen, C. Lee, C.-C. Hsu, Towards developing a matrix-assisted laser desorption/ionization mass spectrometry imaging (MALDI MSI) compatible tissue expansion protocol, Anal. Chim. Acta 1297 (2024) 342345, https://doi.org/10.1016/j.aca.2024.342345.
[71] Y.H. Chan, K.C. Pathmasiri, D. Pierre-Jacques, M.C. Hibbard, N. Tao, J.L. Fischer, E. Yang, S.M. Cologna, R. Gao, Gel-assisted mass spectrometry imaging enables sub-micrometer spatial lipidomics, Nat. Commun. 15 (2024) 5036, https://doi.org/10.1038/s41467-024-49384-w.
[72] H. Zhang, L. Ding, A. Hu, X. Shi, P. Huang, H. Lu, P.W. Tillberg, M.C. Wang, L. Li, TEMI: tissue-expansion mass-spectrometry imaging, Nat. Methods 22 (2025) 1051–1058, https://doi.org/10.1038/s41592-025-02664-9.
[73] J.M. Samuel, N.M. Baby, E.D. Mayo, T. Yan, Z. Liang, B.M. Prentice, Examination of lipid distributions in hydrogel-expanded mouse brain tissue using imaging mass spectrometry, Anal. Chim. Acta 1377 (2025) 344629, https://doi.org/10.1016/j.aca.2025.344629.

Yoichi Otsuka is an Associate Professor in the Department of Physics, Graduate School of Science, The University of Osaka, Japan. He received his B.Sc. (2001), M.Sc. (2003), and Ph.D. (2006) in Chemistry from The University of Osaka under the supervision of Prof. Tomoji Kawai, who pioneered nanoscale electrical measurement techniques using atomic force microscopy and investigated the charge-transport properties of DNA. From 2006 to 2015, he worked as a Research Scientist at Canon Inc., where he contributed to the development of analytical imaging technologies, including mass spectrometry and stimulated Raman scattering microscopy. In 2015, he joined Professor Takuya Matsumoto's laboratory in the Department of Chemistry, Graduate School of Science, The University of Osaka, as an Assistant Professor. From 2020 to 2024, he served as a PRESTO Researcher at the Japan Science and Technology Agency. Since 2021, he has been affiliated with Prof. Michisato Toyoda's laboratory in the Department of Physics, Graduate School of Science, The University of Osaka, where he continues to develop ambient mass spectrometry imaging instrumentation based on scanning probe electrospray ionization (SPESI). He also holds an appointment as Associate Professor at both the Forefront Research Center and Department of Chemistry within the Graduate School of Science at the same university. He currently serves on the Editorial Boards of Mass Spectrometry (Tokyo), the Journal of the Mass Spectrometry Society of Japan (MSSJ), and the International Journal of Mass Spectrometry. His awards include the Pathology International High Citation Award (2016), the Best Presentation Award from the Surface Science Society of Japan (2016), the MSSJ Award for Excellent Papers (2017), and the MSSJ Research Award (2020).